energies

MDPI

Article

Modelling and Analysis of Low and Medium-Temperature Pyrolysis of Plastics in a Fluidized Bed Reactor for Energy Recovery

Natalia Wikira [1], Bahamin Bazooyar [2] and Hamidreza Gohari Darabkhani [1,*]

[1] Centre for Renewable and Sustainable Engineering (CRSE), School of Digital, Technologies, Innovation and Business (DTIB), University of Staffordshire, Stoke-on-Trent ST4 2DE, UK; nwikira@eagle.org
[2] Department of Mechanical and Aerospace Engineering, College of Engineering, Design and Physical Sciences, Brunel University of London, Uxbridge UB8 3PH, UK; bahamin.bazooyar@brunel.ac.uk
* Correspondence: h.g.darabkhani@staffs.ac.uk

Abstract: With the growing demand for plastic production and the importance of plastic recycling, new approaches to plastic waste management are required. Most of the plastic waste is not biodegradable and requires remodeling treatment methods. Chemical recycling has great potential as a method of waste treatment. Plastic pyrolysis allows for the cracking of plastic polymers into monomers with heat in the absence of oxygen, allowing energy recovery from the waste. Fluidized bed reactors are commonly used in plastic pyrolysis; they have excellent heat and mass transfer. This study investigates the influence of low and medium process temperatures of pyrolysis on fluidized bed reactor parameters such as static pressure, fluidizing gas velocity, solid movement, and bubble formation. This set of parameters was analyzed using experimental methods and statistical analysis methods such as experimental correlations of changes in fluidized bed reactor velocities (minimal, terminal) due to temperature increases for different particle sizes; CFD software simulation of temperature impact was not found. In this study, computational fluid dynamics (CFD) analysis with Ansys Fluent was conducted for the fluidization regime with heat impact analysis in a fluidized bed reactor (FBR). FBR has excellent heat and mass transfer and can be used with a catalyst with low operating costs. A two-phase Eulerian–Eulerian model with transient analysis was conducted for a no-energy equation and at 100 °C, 500 °C, and 700 °C operating conditions. Fluidizing gas velocity increases the magnitude with an increase of the operating temperature. The point of fluidization could be determined at 1.1–1.2 s flow time at the maximum pressure drop point. With the increase of gas velocity (to 0.5 m/s from 0.25 m/s), fluidizing bed height expands but when the solid diameter is increased from 1.5 mm to 3 mm, the length of the fluidized region decreases. No pressure drop change was observed as the fluidized bed regime was maintained during all analyses. The fluidization regime depends on gas velocity and all the applied fluidization gas velocities were of a value in between the minimal fluidization velocity and the terminal velocity.

Keywords: plastic pyrolysis; plastic circular economy; fluidization regime; CFD; fluidizing bed reactor; Eulerian–Eulerian model

Citation: Wikira, N.; Bazooyar, B.; Gohari Darabkhani, H. Modelling and Analysis of Low and Medium-Temperature Pyrolysis of Plastics in a Fluidized Bed Reactor for Energy Recovery. *Energies* **2024**, *17*, 6204. https://doi.org/10.3390/en17236204

Academic Editor: Artur Blaszczuk

Received: 30 October 2024
Revised: 27 November 2024
Accepted: 3 December 2024
Published: 9 December 2024

1. Introduction

Plastic waste management is one of the biggest contemporary issues that needs to be addressed. The biggest global plastic recycling rates in 2018 were found in India (60%) and South Korea (45%), followed by European countries (30%), but just 9% of plastic was recycled worldwide. A total of 12% of plastic waste was incinerated, 30% was in use, and 49% was sent to landfills or lost in nature [1]. The most impactful plastic recycling data collected is shown in Figure 1. It shows that just 9% of plastic is recycled worldwide and 49% is sent to landfills or lost in nature [1,2].

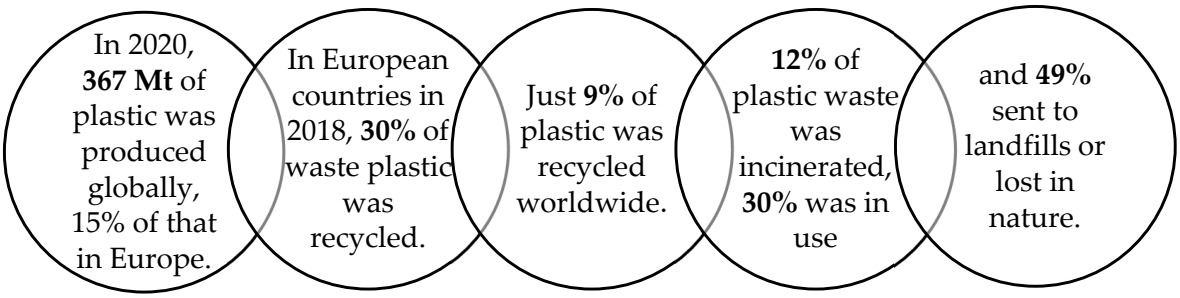

Figure 1. Plastic recycling data (only 9% of plastic is recycled worldwide and 49% is sent to landfills) [1,2].

The aim is for plastic to have an increased economic value for reuse. Reusable plastic products should be promoted before single-use ones and designed with their lifecycle in mind. Plastic must become a renewable resource.

Pyrolysis thermochemical treatment is a technology that has great potential to reduce the amount of plastic waste that goes to landfills or is lost in nature. Not only does it allow us to reuse plastic, but it also allows us to reclaim energy from it. The pyrolysis process allows for the thermal degradation of long-chain polymer molecules of plastic into smaller and less complex ones [3]. Four different mechanisms may occur during the process: random-chain scission, cross-linking, end-chain scission or depolymerization, and chain stripping [4].

Fluidized bed reactors (FBRs) are commonly used reactors in plastic pyrolysis experiments and simulations as they produce uniform yield quality. Fluidized bed reactors have excellent heat and mass transfer and can be used with a catalyst with low operating costs. They provide an efficient and sustainable process of plastic pyrolysis.

FBRs have been used in many processes in the chemical, petrochemical, environmental, energy, and metallurgical industries. Li, et al. list such processes as "fossil fuel combustion, coal and biomass gasification, and fluid catalytic cracking" [5], while Khan, et al. add the following processes: "Olefin polymerization (propylene and ethylene), a wide range of synthesis reactions, manufacturing of silicon, gasoline synthesis (Fischer-Tropsch), coking (Fluid and Flexi)" [6]. Feedstock is introduced into the system through a feeding system, and for plastic pyrolysis a screw feeder usually transports the plastic into the reactor.

Computational fluid dynamics (CFD) software simulations are often used in reactor modeling. Much work on heat transfer in fluidized bed reactors has been conducted [7–9]. Utwitzone et al. focused on solid hold-up in the reactor riser in the pyrolysis process [10]. CFD simulations have also been used with plastic pyrolysis or gasification process chemical kinetics modeling [11,12].

In 2005, Chiesa et al. recognized Eulerian–Eulerian and Eulerian–Lagrangian approaches used in fluidized bed reactor bubble simulations to have similar patterns [13]. While most of the work in CFD analyses of the fluidized bed riser is conducted using the Eulerian–Lagrangian method—such as Khawaja and Shao et al.'s work on the minimal fluidizing velocity changes analyzed from CFD simulation [14,15]—as it requires less computational time, this analysis will use the Eulerian–Eulerian method known as well as the two-fluid model method.

Computational fluid dynamic software simulations are a relatively new approach that allows for the visual and numerical simulation of complex problems. While much work has been conducted on the optimization of the pyrolysis process and fluidizing bed reactor modeling, CFD allows for further improvement. Thanks to CFD, it is possible to troubleshoot reactor parameters and performance before manufacturing.

This paper aims to study the influence of low and medium-temperature pyrolysis processes on fluidized bed reactor parameters such as static pressure, fluidizing gas velocity, solid movement, and bubble formation. This analysis will allow us to visualize the impact on the parameters of the reactor through computational fluid dynamics software. While this set of parameters was analyzed using experimental methods and statistical analysis,

CFD software simulation was not used to study the impact of the process temperatures. Hagh-Shenas-Lari and Mostoufi analyzed pressure changes using statistical analysis [16]. Seo et al. created experimental correlations in changes in fluidized bed reactor velocities (minimal, terminal) due to temperature increases for different particle sizes [17]. This analysis simulated the impact of operating conditions at 100 °C, 500 °C, and 700 °C in a fluidized bed reactor. Set values are below the melting points for most of the polymers and are used for low and medium-temperature pyrolysis processes.

2. Materials and Methods

With the growing demand for plastic production and the importance of plastic recycling, new approaches to plastic waste management are required. Most plastic waste is not biodegradable and requires remodeling treatment methods.

Plastic waste pyrolysis is a chemical recycling process that works by cracking organic materials at high temperatures in the absence of oxygen. Pyrolysis yields include oil, gas, and char. Yield can be used for a new plastic material or as an energy source. Since plastic is a highly calorific product, ranging from approx. 18,000 to 38,000 kcal/kg, it can be considered excellent for energy recovery [18].

Thermal pyrolysis degradation of organic material takes place at different temperatures from 300 °C to 900 °C in the absence of oxygen [19]. Due to the process taking place in an atmosphere not containing an adequate amount of oxidizing agent, combustion does not take effect, and raw material decomposes due to pressure and temperature [20]. Pyrolysis types are briefly described in Figure 2.

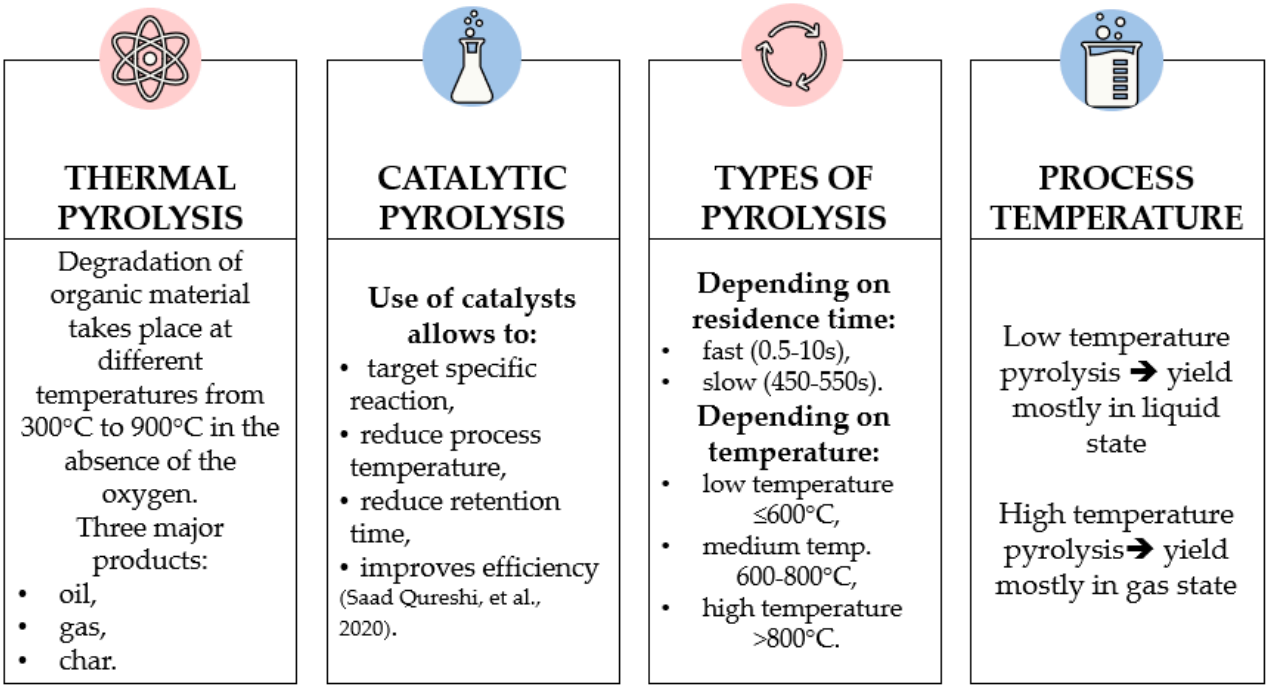

Figure 2. Thermal and Catalytic pyrolysis and types of pyrolysis based on the process parameters (e.g., residence time and temperature) [19].

Depending on temperature, pyrolysis is as follows:

- Low temperature ≤ 600 °C;
- Medium temperature 600–800 °C;
- High temperature > 800 °C.

Thermal plastic pyrolysis, which can be found in industry applications, takes place at a low temperature range (around 500–550 °C) with yields in the form of liquid or wax [21]. Yield in the next stage can be refined into chemicals or fuels [19].

As for the use of catalysts, the best are fluidized bed reactors, which reduce operating costs due to catalyst reuse. They also have high heat transfer rates, well-established temperature control, and solid particle residence time control but are more expensive to set up [22].

Fluidized bed reactors work by utilizing a physiochemical phenomenon called fluidization. In fluidization, a fine, granular material (typically sand) is converted from a solid state into a fluid-like state by the passage of fluid through it.

With an increase in the fluid velocity rate, particles rearrange their space into an expanded bed. Particles get suspended in the fluid at higher velocities. In the suspended form of the bed, the buoyancy force is balanced between gravitational and drag forces, and the pressure drop through any section of the bed is equal to the weight of the particles. The bed is considered fluidized at minimum fluidization velocity (Figure 3) [6,23].

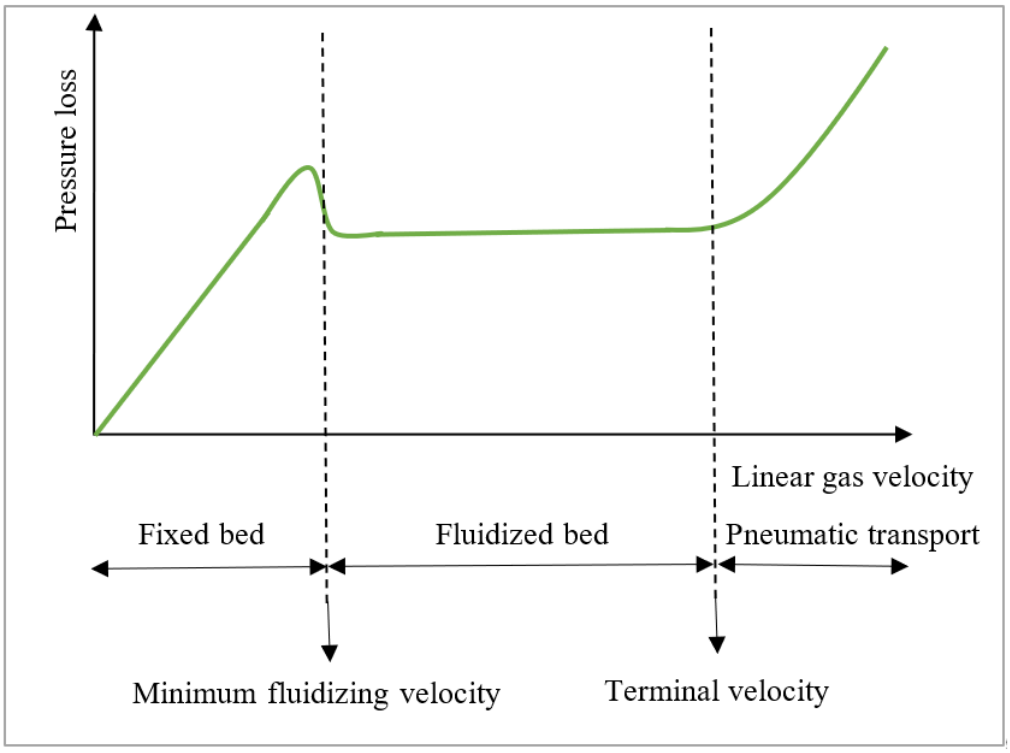

Figure 3. Types of pyrolysis with process parameters. Depending on the minimum fluidizing velocity value fluidization regime is behaving as a fixed bed, fluidized bed or after terminal velocity is reached pneumatic transport occurs.

At minimum fluidization velocity, the pressure drop is stabilized for a certain range of velocities, after which an increase of velocity results in drastic pressure drop change. At higher flow rates, particle movement becomes more vigorous, and bubbles are formed.

With the further increase of the liquid velocity, the bed turns into a turbulent fluidized bed; velocity is then called terminal velocity. This phenomenon leads to the disappearance of the dense phase. Terminal velocity can be applied in fast fluidization.

Types of pyrolysis with process parameters. Depending on the minimum fluidizing velocity value fluidization regime is behaving as a fixed bed, fluidized bed or after terminal velocity pneumatic transport happens

For good fluidizing conditions and solids, run-off prevention of superficial velocity must be maintained. Superficial velocity should be of a value between minimal fluidizing velocity and terminal velocity.

The Eulerian–Eulerian (EE) approach defines the solid and liquid phases as a continuum and phases are modeled as interpenetrating fluids. Conservation equations for mass, momentum, and energy are solved for each phase. The Eulerian–Eulerian model

is known as well as two-fluid model (TFM). Both phases coexist everywhere in the flow domain. The portion of volume occupied by a phase is given by the volume fraction. The phase-coupled SIMPLE method was used for the solution method, where "the velocities are solved coupled by phases in a segregated fashion. Fluxes are reconstructed at the faces of the control volume and then a pressure correction equation is built based on total continuity. The coefficients of the pressure correction equations come from the coupled per phase momentum equations" [24].

Most simulations of fluidized reactor riser flows are carried out with a two-dimensional flow assumption with a plane cutting along the axis of the cylindrical column [5]. Reactor material is proven to have a negligible effect on thermal properties and reaction parameters inside the reactor and was left in the default setting [25].

The 2D geometry of the modeled fluidized reactor riser was created as a cylinder of 1.2 m in height with a uniform diameter of 0.2 m as shown in Figure 4. DesignModeler was used as computer-aided design software to create the geometry.

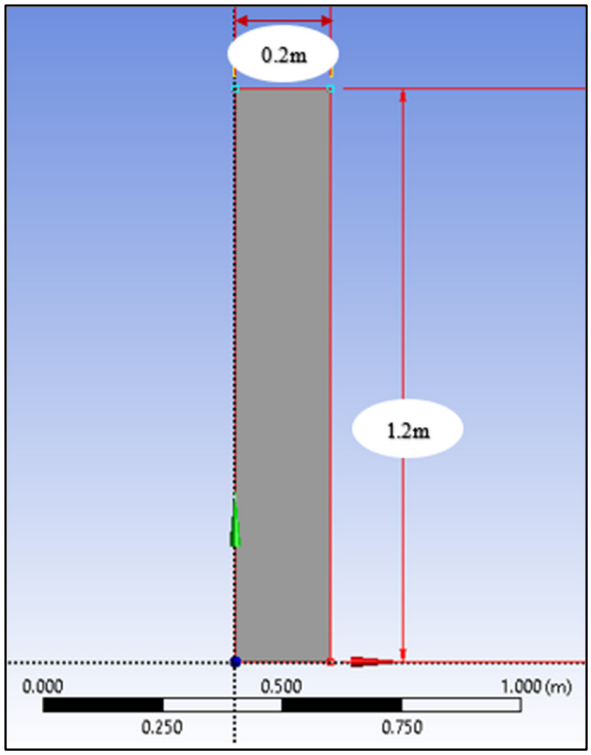

Figure 4. The 2D geometry of the modeled fluidized reactor riser of 1.2 m in height and a uniform diameter of 0.2 m.

A face meshing method was employed using quadrilateral-shaped elements, with the mesh elements being nearly uniform in size and shape, as illustrated in Figure 5. Mesh element quality was checked with an excellence score. Aspect ratio is the ratio of the longest edge length to the shortest edge length and can be understood as a measure of the stretching of the mesh element. The aspect ratio of 1, indicating an ideal square, was obtained for an average value. Skewness shows the difference between the shape of the mesh cell and the shape of an equilateral cell of equivalent volume. Values of skewness come from the range 0–1; accuracy is decreased as the skewness value gets closer to 1 and the solution is destabilized. The model shows the average value of 1.307×10^{-10} of the skewness mesh metric. The ideal value for skewness is zero. Mesh shape should not have an impact on the quality of the results, but the element size should be investigated as it is bigger (3 times) than the value recommended in the literature. It is expected that the grid size should be around 10 times the size of the particle diameter [5,6].

Element size was set to 0.005 m, creating 9600 elements with 9881 nodes. Optimal mesh element size in fluidized bed reactors depends on the diameter of the solid particles and this analysis was performed for silica sand of 0.00015 m diameter.

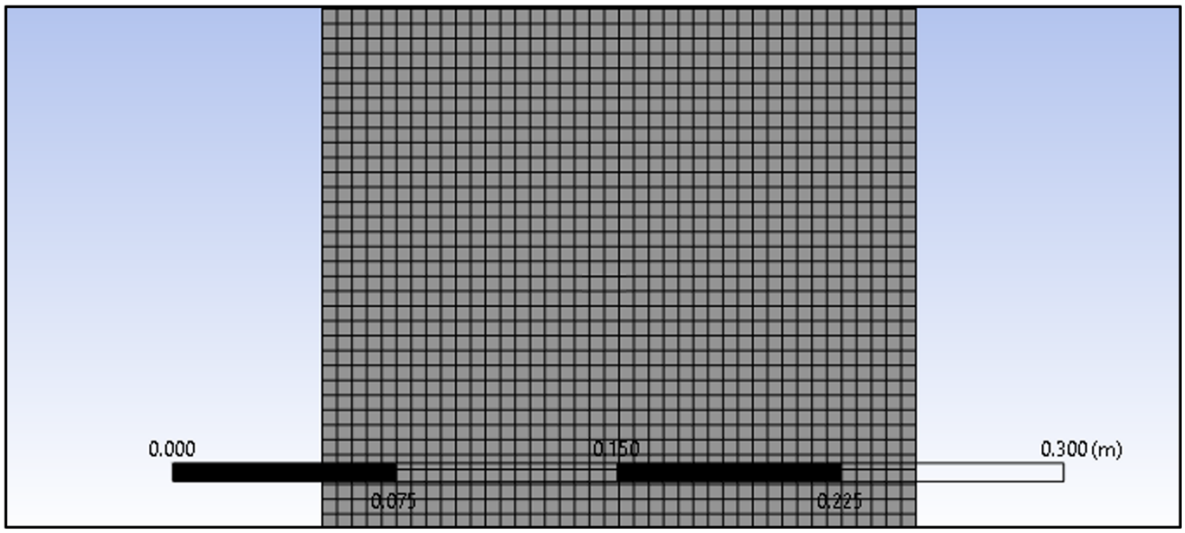

Figure 5. Structured mesh with a 0.005 m element size and 9600 elements.

Fluidization regime analysis was created to inspect the basic regime parameters in the reactor riser. Analysis was conducted to check the impact of the increased pyrolysis temperatures, with the reactor operating at 100 °C, 500 °C, and 700 °C. A second analysis was performed to show the impact of the increase in the fluidizing velocity and solid diameter. Analyses were conducted with Double Precision and 4 Solver processes in Ansys Fluent 2020 R1 software. The basic parameters of the carried analyses are shown in Figure 6.

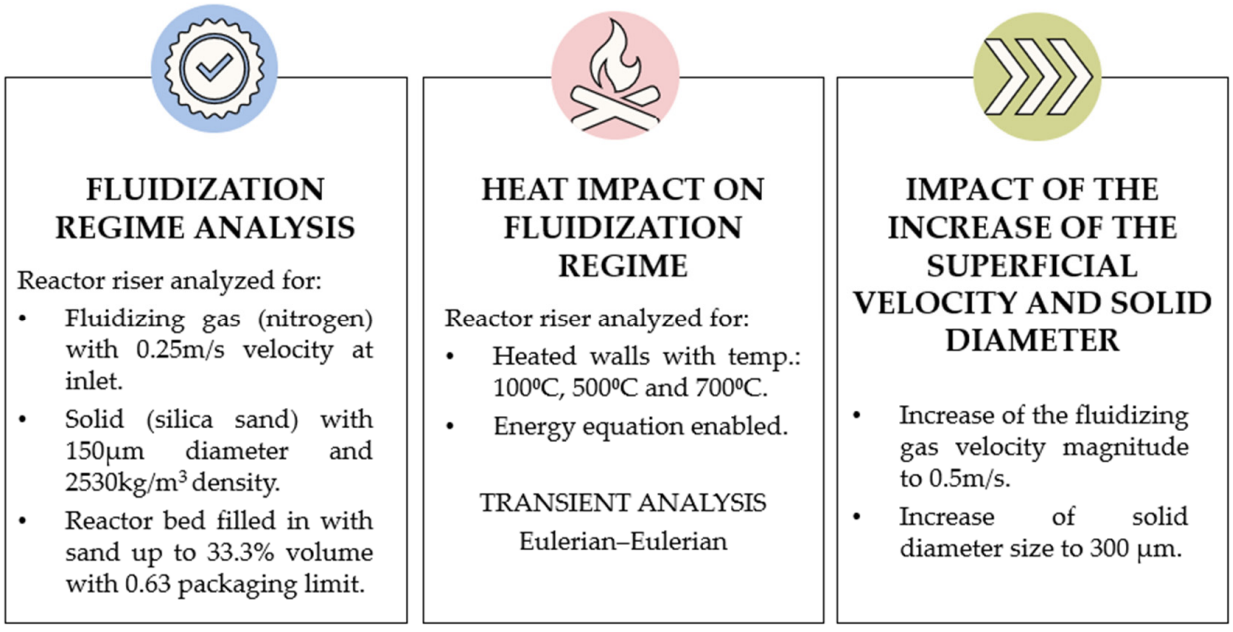

Figure 6. Main parameters of carried simulations for heat impact on the fluidization regime as well as the impact of the increase in gas superficial velocity and solid diameter on the riser bed height.

The settings used in analyses were collected and are shown in Table 1. Pressure-based, transient analysis with a standard viscous model was performed. SIMPLE scheme velocity–pressure coupling was chosen.

Table 1. Basic analysis settings used in flow regime and heat impact analyses.

Time	Transient
Scenario type	Pressure-based (incompressible flow)
Viscous Model	Standard k-ε, standard wall functions
Gravitational acceleration	9.81 m/s^2
Velocity-pressure coupling	SIMPLE scheme
Operating pressure	101,325 Pa
Outlet gauge pressure	10,1325 Pa
Solution methods	Pseudo transient
Initialization	From inlet
Number of time steps	400
Time step size	0.01 s

To analyze the fluidizing regime, a Eulerian two-phase system was used. Two phases were decided upon: fluidizing gas (nitrogen) and solid (silica sand). The primary gas phase was set as nitrogen with the parameters available in the software database. The secondary phase was created as silica sand with a granular diameter of 0.00015 m. These settings and more were collected and are shown in Table 2.

Table 2. Basic analysis settings used in flow regime and heat impact analyses.

Drag model	Syamlal–O'Brien
Sand granular viscosity	Syamlal–O'Brien
Granular bulk viscosity	Lun-et-al
Packing limit	0.63
Sand density	2530 kg/m^3
Sand mean diameter	0.00015 m
Calculated minimal fluidizing velocity	0.05379 m/s

The time step has an important effect on the accuracy of bubble simulation. Computational time is usually affected by the time step size; the smaller the time step, the longer it takes to obtain results for a set amount of time. But the smaller the time step, the more accurate the results are.

To assess time step size, the Courant number can be used. The Courant number should be kept small to achieve better accuracy. The Courant number can be interpreted physically as the ratio of the distance traveled in one time step to the mesh spacing.

The Courant number was assured to be $\leq$1 (a requirement for boundedness).

The solution reached convergence in between time steps for the default value of residuals.

The drag force of upward moving gas must be equal to the weight of particles for minimum fluidization velocity to occur. Due to its high density and weight, silica sand is used as a heat-transferring medium in plastic pyrolysis. Analyzed sand has a density of 2530 kg/m^3, while HDPE at 20 °C has a density of 960 kg/m^3 [26], and at 500 °C, 830 kg/m^3 [27].

In the article 'An Assessment of Drag Models in Eulerian–Eulerian CFD Simulation of Gas-Solid Flow Hydrodynamics in Circulating Fluidized Bed Riser' by Upadhyay, et al., the Syamlal–O'Brien drag model was found to be the most accurate [28]. The Syamlal–O'Brien drag model for FBR was also suggested by Khan, et al. when using the Eulerian multiphase model [6].

The superficial fluidizing velocity used in fluidized bed reactors is usually of 3 times (up to 8 times) the value of the minimal fluidization velocity [29,30]. In this analysis, superficial velocity was set to 0.25 m/s (4.65 times the calculated minimal fluidization velocity).

Two additional analyses were completed for the fluidizing gas velocity increase to 0.5 m/s and solid diameter increase to 0.0003 m (twice the initial values) to simulate the impact of these changes on the dense bed.

The heat impact on fluidizing regime analysis was examined at three different temperatures: 100 °C, 500 °C, and 700 °C, and additional parameters are shown in Tables 3 and 4.

Table 3. Additional parameters used in heat impact analyses.

Energy equation	on	
Sand granular temperature	m^2/s^2	1×10^{-5}
Sand specific heat	J/kg K	737 *
Heat transfer coefficient (between nitrogen and silica sand)	W/(m^2 K)	Gunn model

* Quartz SiO_2 has a specific heat of 742.13 J/kg K [31].

Table 4. Additional parameters used in heat impact analyses.

Zone		Additional Information	Temperature [K]	Temperature [K]	Temperature [K]
Velocity inlet	sand	No fraction	293	293	293
	nitrogen	Velocity 0.25 m/s			
Pressure outlet	sand	No backflow	293	293	293
	nitrogen				
Walls (stationery wall)			373.15	773.15	973.15
Operating conditions			373.15	773.15	973.15

The typical range of the solid volume in fluidized bed risers is ≤40% of the total volume [32]. For this analysis, the created region takes 33.3% of the total volume.

3. Results

3.1. Sand Volume Fraction and Fluidizing Gas Velocity

The 4 s flow regime was analyzed at different operating conditions. Sand fraction contours were obtained with no energy equation and at working conditions of 100 °C, 500 °C, and 700 °C. Figures 7–10 show the movement of the volume fraction in time. In the first second of the flow regime (before the point of fluidization), gas can be seen not leaving the sand fraction. The fluidization regime is stabilizing with the flow time passing and the formation and movement of bubbles can be seen.

The height of the fluidizing bed does not depend on operating temperature but on superficial fluidizing gas velocity; as only one velocity value of 0.25 m/s was used in the analysis all developed beds have similar heights. The volume fraction of sand after 1 s of flow time has a lower height than after the point of fluidization (maximum pressure drop at 1.2 s). When running analysis without an energy equation, smaller bed height is acquired.

Behind gas bubbles, a wake with a solid is observed, with bubble movement promoting gas and sand mixing. The intensity of this mixing depends on bed size and gas velocity, and it is higher in large fluidizing beds and at higher fluidizing velocities [33]. The surface of the fluidized bed is not straight and is horizontal as rising gas bubbles burst to reach the surface.

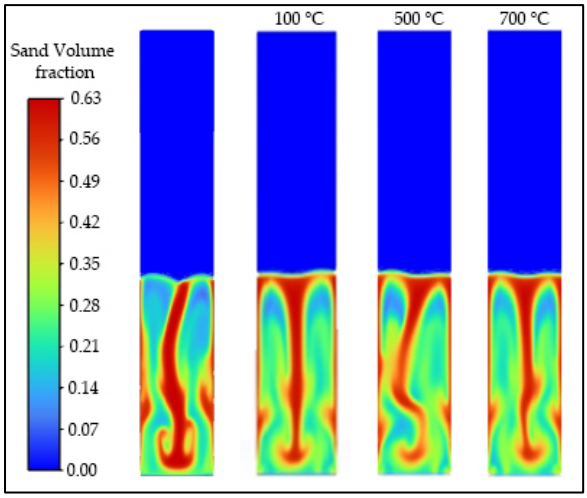

Figure 7. Sand fraction contours after 1 s of flow time with no energy equation and at working conditions of 100 °C, 500 °C, and 700 °C.

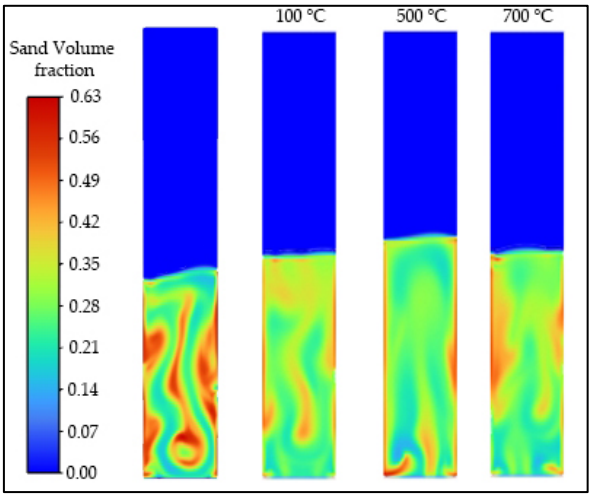

Figure 8. Sand fraction contours after 2 s of flow time with no energy equation and at working conditions of 100 °C, 500 °C, and 700 °C.

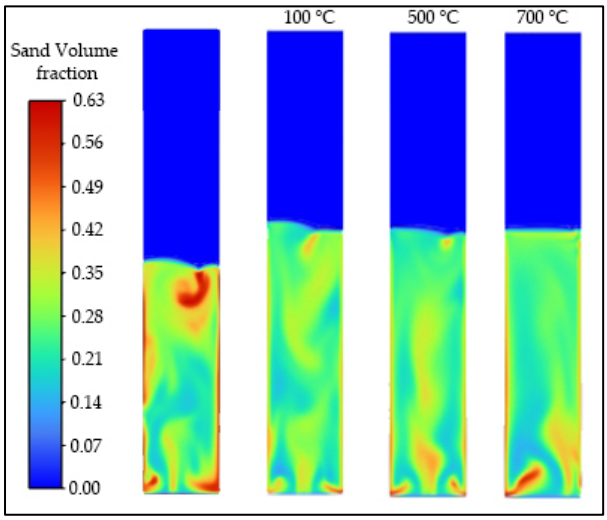

Figure 9. Sand fraction contours after 3 s of flow time with no energy equation and at working conditions of 100 °C, 500 °C, and 700 °C.

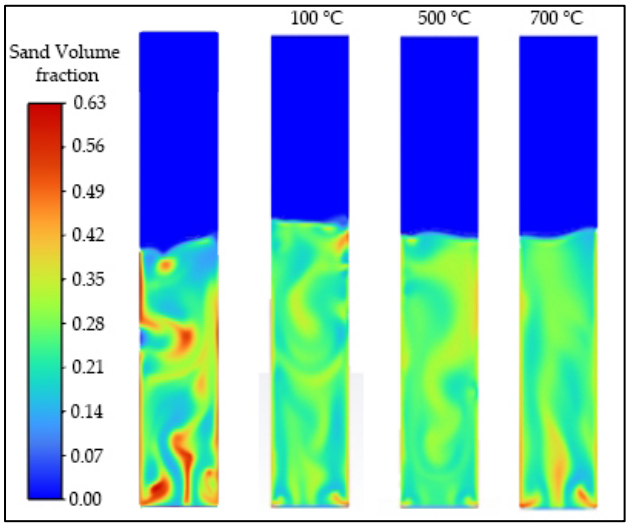

Figure 10. Sand fraction contours after 4 s of flow time with no energy equation and at working conditions of 100 °C, 500 °C, and 700 °C.

The axial solid hold-up is denser near the bottom region of the riser and more scattered in the top region of the riser for all working conditions. A typical L-shaped profile was acquired [22]. The upward movement of the bubbles can be seen. The mixing of solids is affected by the collision and coalescence of bubbles. Bubble diameter, and the distribution of bubbles and their collision are important parameters in fluidization [6].

The impact on the solid bed height of an increase in velocity from 0.25 m to 0.5 m/s was simulated (with a constant 0.00015 m solid diameter) as well as for an increase in solid diameter from 0.00015 m to 0.0003 m (with a constant value of superficial velocity of 0.25 m/s).

With doubled gas velocity, a sharp increase in fluidizing bed height is seen, the flow becomes more turbulent, and bubbles are more combined. A reverse effect was obtained with an increase in solid diameter. Both effects on the dense bed height, of changes in velocity and solid diameter, can be seen in Figure 11. An increase in the fluidizing gas velocity increases the dense bed height while the increase in solid diameter reduces it. The pneumatic flow was not reached with this velocity increase.

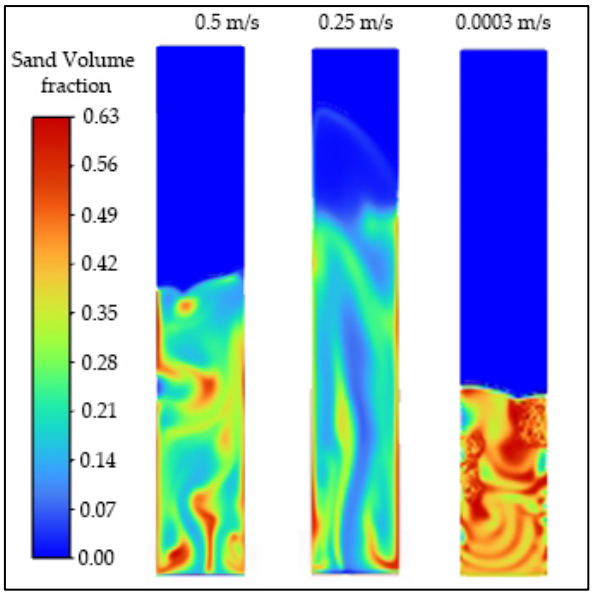

Figure 11. Changes in the bed size for the superficial velocity of 0.25 m/s and 0.5 m/s magnitude (simulated for the initial value of a solid diameter of 0.00015 m) and increase in solid diameter from

0.00015 m to 0.0003 m (with a 0.25 m/s fluidizing gas velocity) in 4 s of the flow time. An increase in the fluidizing gas velocity increases the dense bed height while the increase in the solid diameter reduces it. The pneumatic flow was not reached with this velocity increase.

The 4 s flow regime was analyzed for different operating conditions. Gas velocity contours were obtained with no energy equation and at working conditions of 100 °C, 500 °C, and 700 °C as seen in Figures 12 and 13.

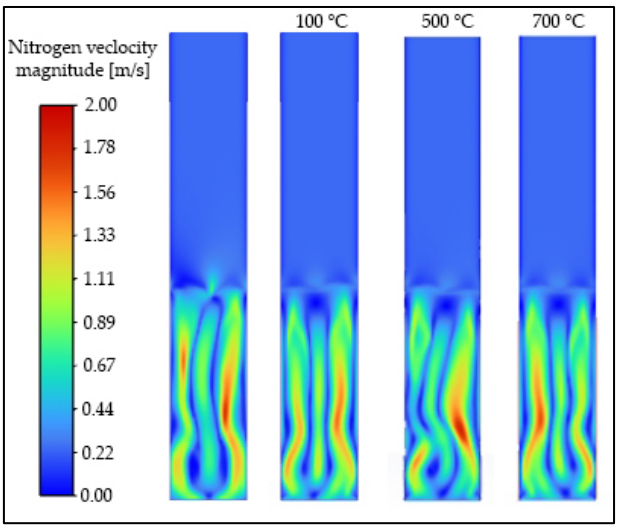

Figure 12. Gas velocity contours after 1 s of flow time before reaching the fluidization point with no energy equation and at working conditions of 100 °C, 500 °C, and 700 °C.

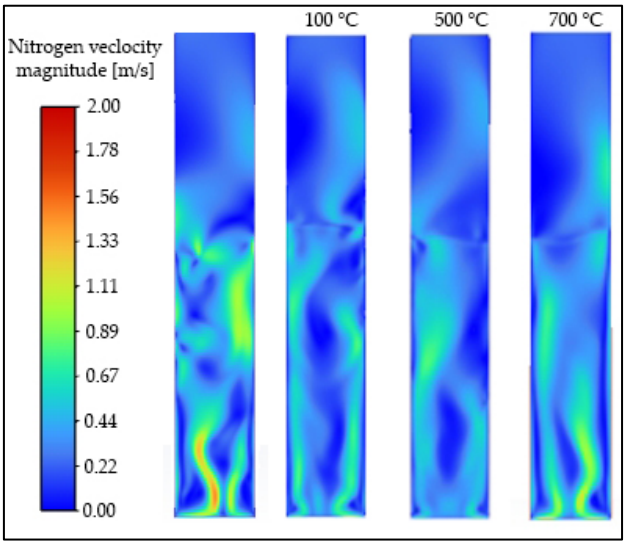

Figure 13. Gas velocity contours after 4 s of flow time with no energy equation and at working conditions of 100 °C, 500 °C, and 700 °C.

Nitrogen gas velocity has the highest magnitude at the initial (1 s) stage out of the materials examined. When the energy equation was included in the analysis, the impact of the temperature increase could be seen on the velocity contours. Velocity has a bigger magnitude at higher operating temperatures.

Velocity in the fluid domain has dominating values below 0.3 m/s in all simulations. When increasing the operating temperature of the system, higher maximum velocities were shown on the histograms. At 100 °C, the maximum value was 0.86 m/s at 500 °C and 1.13 m/s at 700 °C operating temperature, and fluidizing gas velocity went up to 1.25 m/s

in the fluid domain after 4 s of flow time. Velocity magnitude histograms can be seen in Figures 14 and 15.

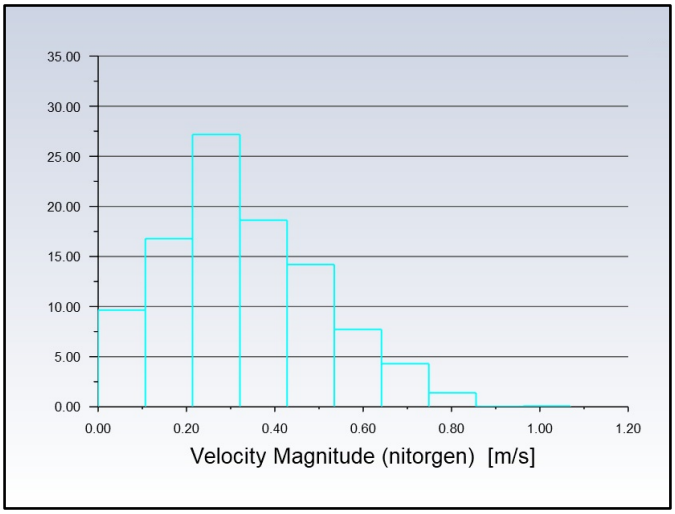

Figure 14. Velocity magnitude histogram after 4 s of flow time in a fluid domain at 100 °C operating conditions. Between 0.21 and 0.32 m/s for 27.12%. Between 0.32 and 0.43 m/s for 18.64%.

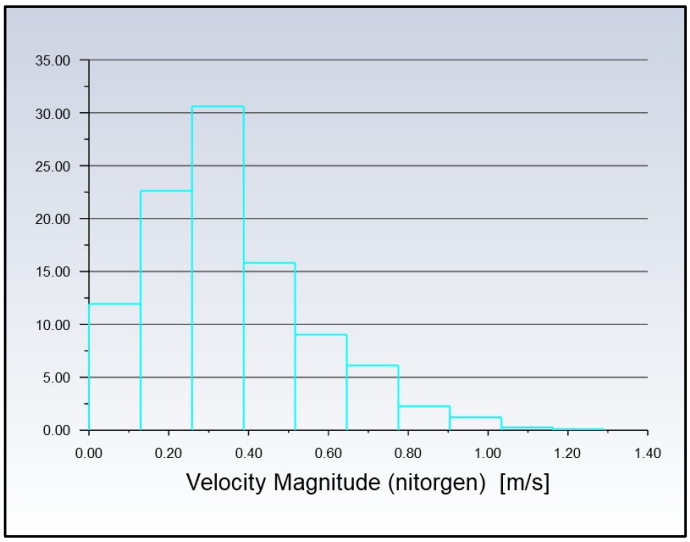

Figure 15. Velocity magnitude histogram after 4 s of flow time in a fluid domain at 700 °C operating conditions. Between 0.26 and 0.39 m/s for 30.60%. Between 0.13 and 0.26 m/s for 22.63%.

3.2. Static Pressure and Pressure Drop

Static pressure contours were created with no energy equation and at working conditions of 100 °C, 500 °C, and 700 °C as seen in Figure 16.

An increase in the velocity with operating temperature did not influence static pressure. In fluidized bed reactors, static pressure has the highest value at the bottom of the bed and decreases as the height increases. Figure 17 was created with the collected data in this analysis.

The point of fluidization can be observed around 1.1 s of flow time without an energy equation, and around 1.2 s for 100 °C, 500 °C, and 700 °C operating temperatures. The point of fluidization can be determined from the maximum pressure drop in the riser, after which the force of the pressure drop multiplied by the cross-section is equal to the weight of the silica sand particles [34]. With constant fluidizing velocity, the pressure drop is expected to be constant in value and does not change with operating temperature change.

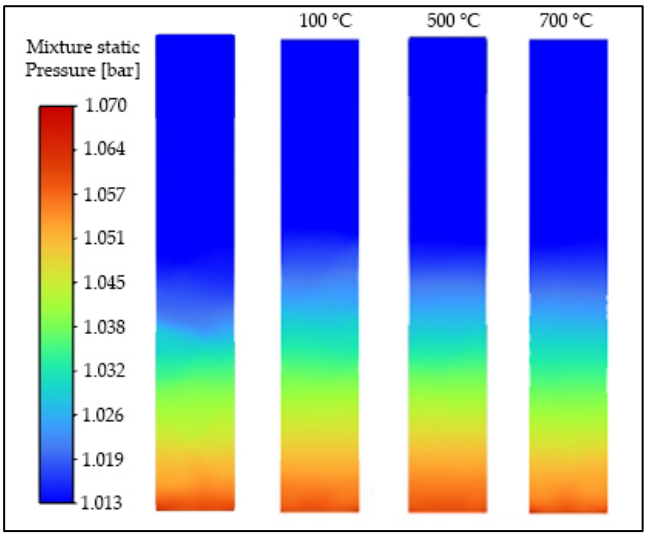

Figure 16. Static pressure contours after 4 s of flow time, showing similar patterns and values of static pressure for all simulations, with no energy equation and at working conditions of 100 °C, 500 °C, and 700 °C.

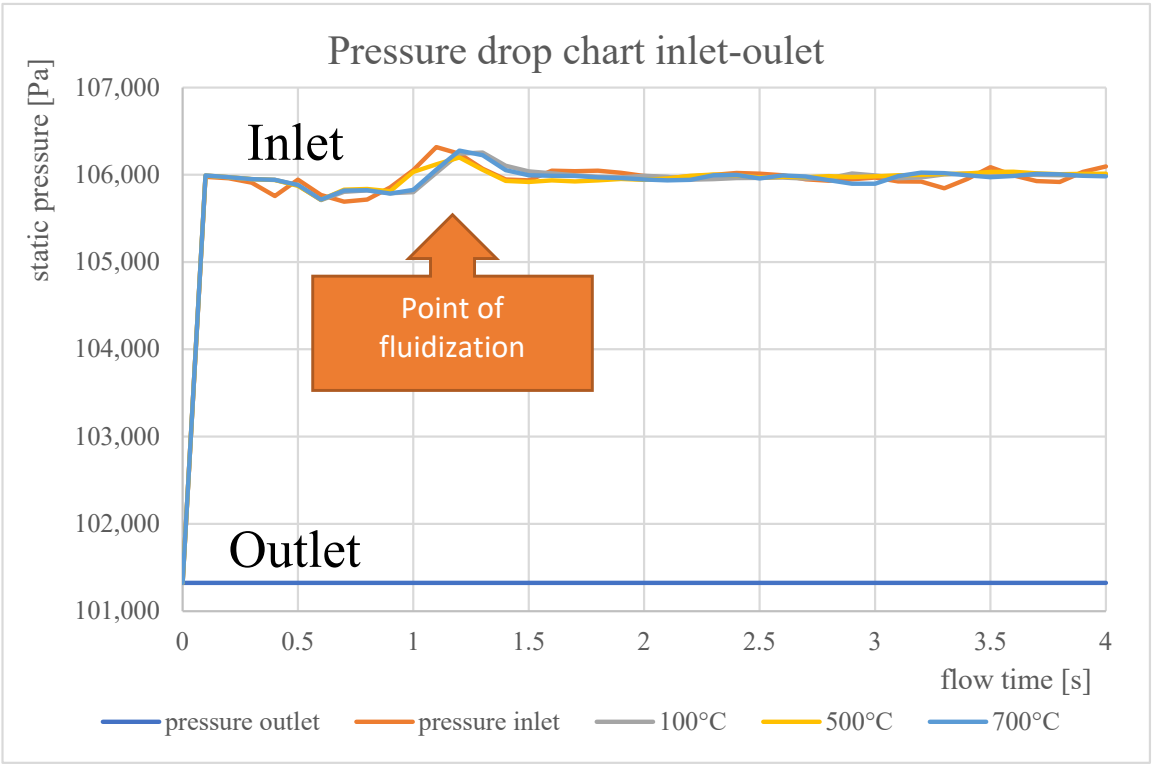

Figure 17. Pressure drop chart between inlet and outlet simulated with no energy equation (pressure inlet) and at operating temperatures of 100 °C, 500 °C, and 700 °C. Pressure at the outlet in all simulations was equal to the atmospheric pressure.

In Figure 18, the impact of increased fluidizing gas velocity from the initial value of 0.25 m/s to 0.5 m/s and an increase in solid diameter from 0.00015 m to 0.0003 m on pressure drop can be seen. For analysis of the increased diameter, the plot stabilization method would be advised. All plots can be considered of similar value. At approximately 2.75 s of flow time, all plots get stabilized. The constant value of the pressure drop is expected after that point in time for all simulated scenarios. Parameter changes did not change the fluidization regime thanks to which the average value of the pressure drop did

not increase or decrease in all simulations. The outlet was calibrated to the atmospheric pressure value of 1013 hPa to show the difference in the process parameters with regard to the standard pressure at sea level.

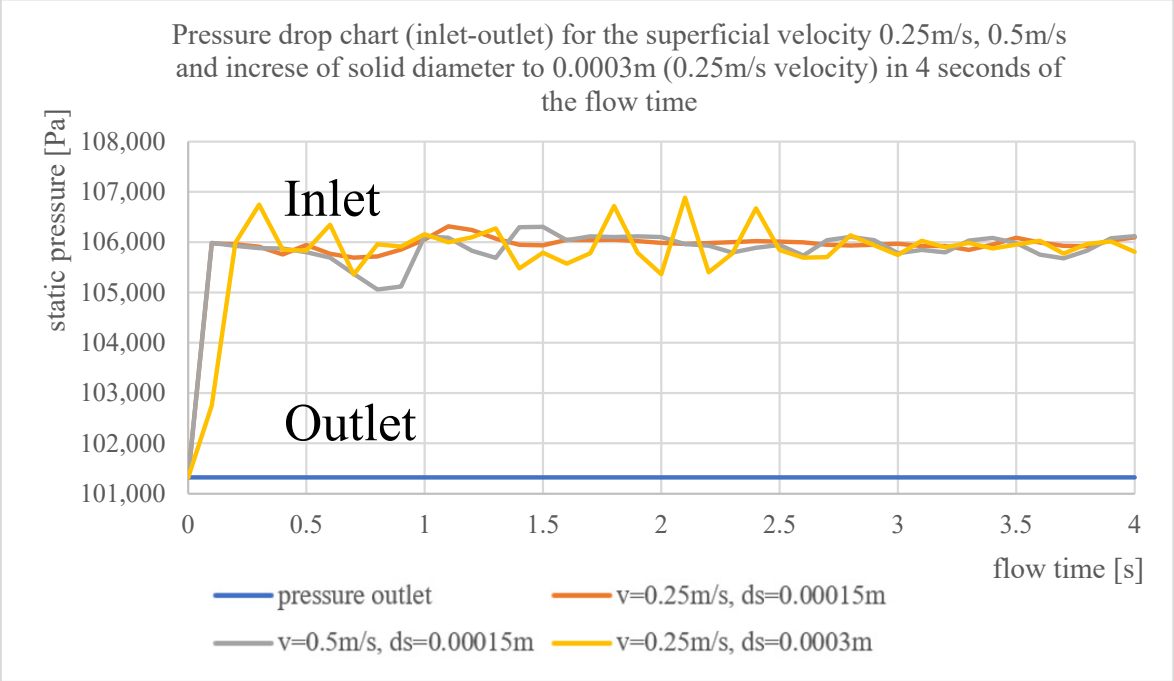

Figure 18. Pressure drop chart inlet–outlet for the superficial velocity of 0.25 m/s, 0.5 m/s magnitude (simulated for the initial value of solid diameter), and increase in solid diameter from 0.00015 m to 0.0003 m (0.25 m/s velocity) in 4 s of the flow time. Pressure at the outlet in all simulations was equal to the atmospheric pressure.

3.3. Grid Independence Study

The smaller grid has better accuracy and requires longer CPU time (Table 5).

Table 5. Grid size impact on CPU time of solving 4 s of flow time simulation without an energy equation. Data was acquired from Ansys software. Reducing the element size used in this analysis to a literature value of 10 times the solid diameter size would gain an additional 5 h of CPU time for each analysis.

Grid Size	10 ds	20 ds	33 ds	40 ds	50 ds
Element size	0.0015 m	0.003 m	0.005 m	0.006 m	0.0075 m
CPU time	6 h 17 min	2 h 33 min	1 h 13 min	15 min	15 min

A grid independence study was conducted with regard to "CFD simulations of circulating fluidized bed risers, part I: Grid study" by Li, et al. [5]. That study found that the smaller grid had the same volume fraction pattern but bigger volume and velocity values compared to a bigger grid size.

In this study, the sand fraction can be seen creating solid hold-up next to the walls in all simulations (Figure 19). One region of additional volume (curvature in the Figure 19 plot) can also be observed at a similar distance along the riser in all analyses giving a good approximation of the layer positioning. The impact on the bed volume can be seen in Figure 20.

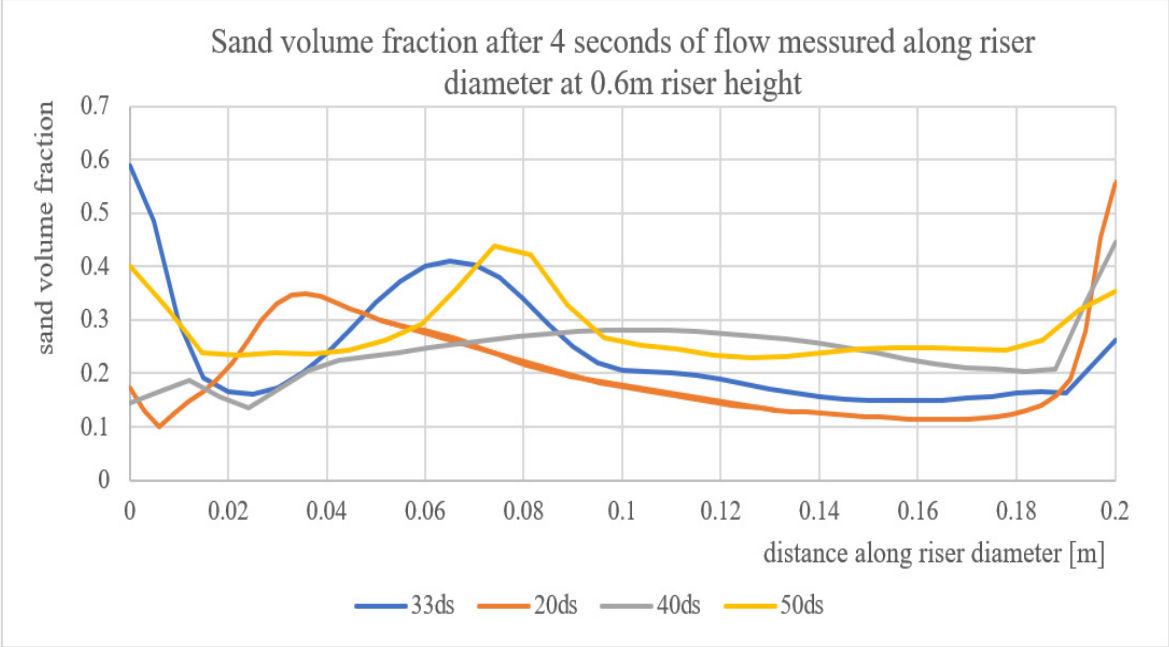

Figure 19. Sand volume fraction after 4 s of flow simulation measured along the riser diameter at 0.6 m height (for the full length of 0.2 m riser diameter) for different grid sizes (20, 33, 40, and 50 times the solid diameter size).

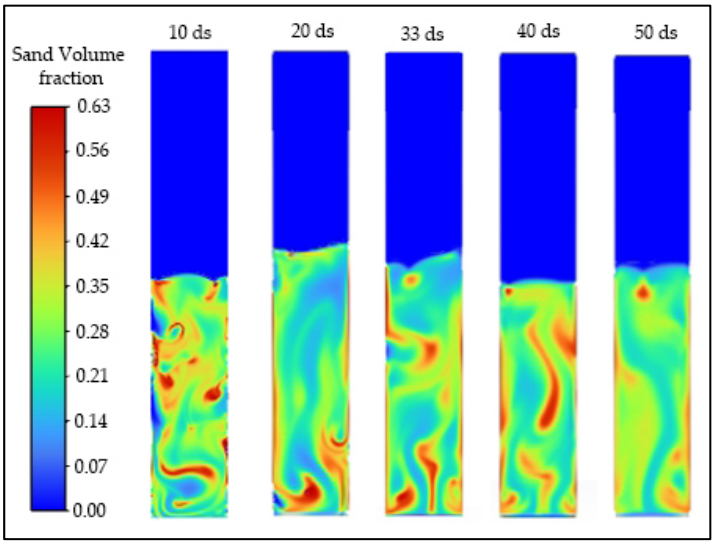

Figure 20. Sand volume fraction after 4 s of simulation for different grid sizes (10, 20, 33, 40, and 50 times the solid diameter size).

In Figure 19, sand volume fractions after 4 s of flow time can be seen for different grid sizes. Different grid sizes, with the rest of the simulation parameters being the same, give different bed sand volume fraction patterns. The literature advises a size of 10 times the solid diameter, showing most specified bubble structures with mixing and solids in their wake as seen in Figure 20. It would be advised to use a 10 ds grid size, but this would require an increase in CPU time.

The pressure drop for different element sizes was examined and data was used to create Figure 21. The smallest grid size of 10 ds gives the most fluctuation in the results, with the point of fluidization at around 1 s of flow time (maximum difference in the pressure). The less detailed the grid, the more the inlet static pressure plot is stabilized.

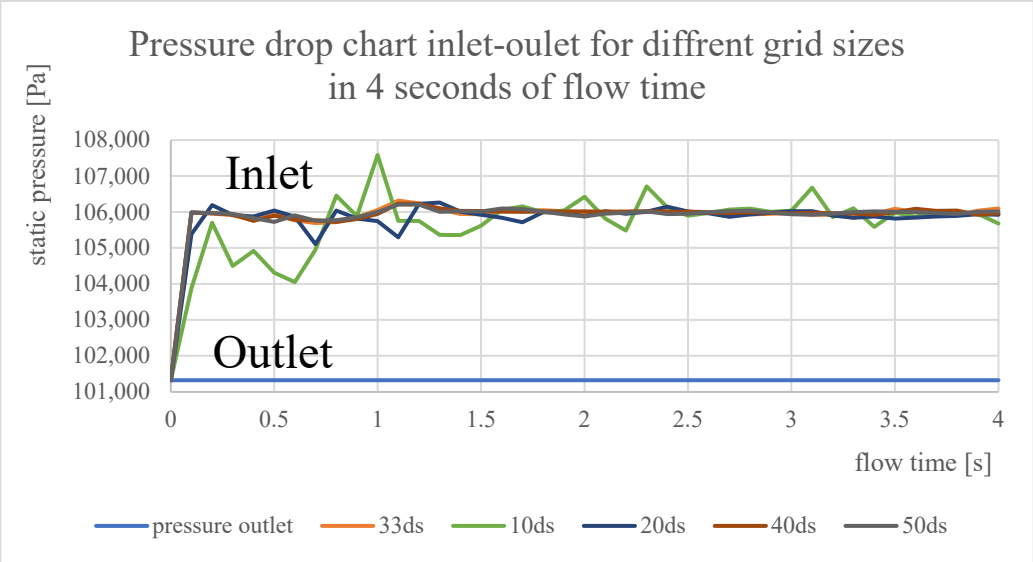

Figure 21. Pressure drops between the inlet and outlet for different grid sizes (33, 10, 20, 40, and 50 times the solid diameter) in 4 s of flow time in the reactor. Pressure at the outlet in all simulations was equal to the atmospheric pressure.

The average heat transfer coefficient was monitored through Equation (1) and applied to the custom field function. The created average heat transfer coefficient was used to create a surface report definition at the point surface.

$$htc_{ave} = \frac{-k_{mix} \cdot (t_{mix} - t_{wall})}{A_{wall}} / (t_{wall} - t_{fluid}) \quad (1)$$

The heat transfer coefficient was monitored at 0.3 m bed height on one heated wall as shown in Figure 22.

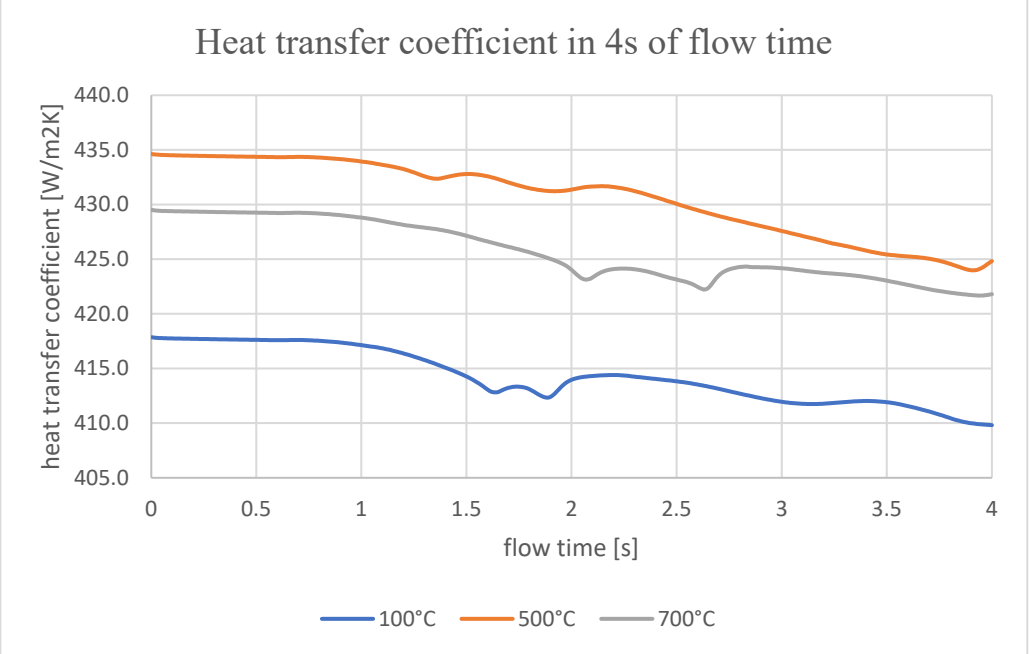

Figure 22. The plot of the heat transfer coefficient next to the heated wall vs. flow time (for mixture average data).

When a solid moves in the wake after gas bubbles, mixing occurs as well as heat transfer. The overall heat transfer coefficient can be used to measure the ability to transfer heat. The heat transfer coefficient is expected to be reduced with exponential distribution, but the time of the flow stabilization was not reached. An imbalance of the plot (fluctuation) was seen due to the fluid mixing.

The heat transfer coefficient was monitored on one heated wall while solid transfer and mixing were taking place, and an imbalance of the plot (fluctuation) is expected to be created from gas movement at that point. They are outcomes of flow regime changes.

For the analyzed solid diameter and bed density, the heat transfer coefficient was expected to be approx. 500 W/m^2 K (Figure 23). The analysis shows that with an increase in operating temperature, the heat transfer value increases.

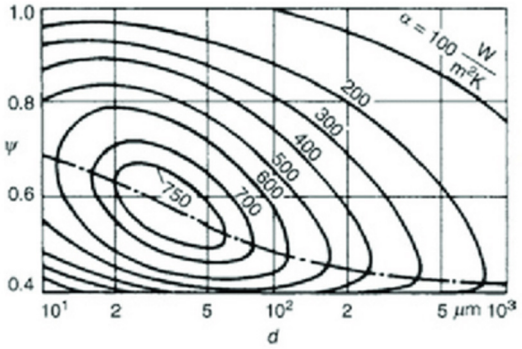

Figure 23. Heat transfer coefficient of a fluidized bed (silica sand) [31].

More heat is transferred when fluidizing velocity is increasing and less when the bed is more densely packed with solids [35]. Particle size has the biggest impact on heat transfer (Figure 23).

4. Discussion

To gain an understanding of the impact of plastic pyrolysis operating temperatures on fluidization regimes, computational fluid mechanics simulation was conducted.

The fluidizing regime analysis was performed. A Eulerian–Eulerian method was used with fluidizing nitrogen gas and a silica sand bed. Analysis was performed for 4 s of flow time. When modeling fluidized bed reactors, the most important parameters to consider are the solid diameter and superficial gas velocity. They decide mixing properties and bubble formation.

Analysis was conducted with no energy equation and at working conditions of 100 °C, 500 °C, and 700 °C. Silica sand parameters were as follows: 2530 kg/m^3 density, 0.00015 m diameter, and 737 J/kg K specific heat. Nitrogen had default system settings. The sand bed had an initial volume that was 33% of the riser. The superficial gas velocity used in the analysis was 0.25 m/s.

When inspecting the contours for the solid volume fraction, the axial solid hold-up can be seen to be denser near the bottom region of the riser and more scattered in the top region of the riser for all working conditions. A typical L-shaped profile was created for the solid movement. The upward movement of the bubbles can be seen with solid movement in the wake.

The operating temperature had an impact on gas velocity and should be considered at the design stage and incorporated in minimal fluidizing velocity calculations. Gas velocity has a bigger magnitude at higher operating temperatures. The point of fluidization could be determined at a 1.1–1.2 s flow time at the maximum pressure drop point further proven by velocity and solid volume fraction contours after 1 s of flow time (fluidizing gas not leaving the surface).

While operating temperature has an impact on the fluidizing gas velocity, in this analysis the fluidization regime was not changed. An increase in the superficial velocity

and solid diameter was proven to have a higher impact on the reactor parameters than temperature. The intensity of mixing depends on bed size and gas velocity, and it is higher in large fluidizing beds and at higher fluidizing velocities. With an increase in gas velocity (from 0.25 m/s to 0.5 m/s with a constant solid diameter of 0.00015 m), fluidizing bed height gets bigger but when the solid diameter is increased (from 0.00015 m to 0.0003 m with a superficial velocity of 0.25 m/s) solid bed height gets smaller compared to the initial analysis. It did not increase or decrease the pressure drop value as the fluidization regime did not change for the analyzed parameters.

A grid independence study was carried out, proving that smaller element sizes should be used for more accurate results, and better bubble formation tracking with higher result accuracy.

5. Conclusions

This study monitored the effects of temperature increases on fluidization regime as well as some process parameters such as increases in superficial velocity and particle diameter. The assumption that the highest process sensitivity is connected to the changes in superficial velocity and solid diameter was proven, showing the necessity of including the process temperature in the superficial velocity calculations for process optimization. Fluidization reactor modeling in Ansys Fluent software allowed for troubleshooting potential limitations due to high process temperatures. Using CFD was shown to be an efficient methodology for process modeling at the early stages of the design.

The analysis of the fluidizing regime was performed with many aspects but more interest in minimal fluidizing velocity would be advised. Minimal fluidizing velocity depends on gas and solid density that change with operating temperature and should be calculated at the design stage. It would be also advised to assess minimal fluidizing velocity with CFD simulation using pressure drop changes vs. superficial velocity charts.

An investigation into the pressure drop plot instabilities at the inlet should be conducted for the increased solid diameter and reduced grid size to assess if these were outcomes of the modeling technology or possible sources of the process disturbance.

A smaller grid of 10 times the size of the solid diameter is recommended for fluidizing the bed reactor design to properly assess mixing and bubble movement and improve the accuracy of results. A bigger grid was used in this analysis to save computational time.

Author Contributions: Conceptualization, H.G.D. and N.W.; methodology, software, validation, formal analysis, investigation, data curation, visualization, and writing—original draft preparation, N.W.; writing—review, editing, and supervision, B.B. and H.G.D. All authors have read and agreed to the published version of the manuscript.

Funding: This research received no external funding.

Data Availability Statement: The original contributions presented in the study are included in the article, further in-quiries can be directed to the corresponding author/s.

Conflicts of Interest: The authors declare no conflicts of interest. The funders had no role in the design of the study; in the collection, analyses, or interpretation of data; in the writing of the manuscript; or in the decision to publish the results.

References

1. Veolia. Plastic Recycling: A Key Link in the Circular Economy. 2018. Available online: https://www.planet.veolia.com/en/plastic-recycling (accessed on 12 April 2022).
2. Plastics Europe, Plastics-the Facts 2021. 2021. Available online: https://plasticseurope.org/knowledge-hub/plastics-the-facts-2021/ (accessed on 12 April 2022).
3. Sharuddin, S.D.A.; Abnisa, F.; Daud, W.M.A.W.; Aroua, M.K.; Sharuddin, A. A review on pyrolysis of plastic wastes. *Energy Convers. Manag.* **2016**, *115*, 308–326. [CrossRef]
4. Gebre, S.H.; Sendeku, M.G.; Bahri, M. Recent Trends in the Pyrolysis of Non-Degradable Waste Plastics ChemistryOpen. *ChemistryOpen* **2021**, *10*, 1202–1226. [CrossRef] [PubMed]

5. Li, T.; Gel, A.; Pannala, S.; Shahnam, M.; Syamlal, M. CFD simulations of circulating fluidized bed risers, part I: Grid study. *Powder Technol.* **2014**, *254*, 170–180. [CrossRef]
6. Khan, M.J.; Hussain, M.A.; Mansourpour, Z.; Mostoufi, N.; Ghasem, N.M.; Abdullah, E.C. CFD simulation of fluidized bed reactors for polyolefin production—A review. *J. Ind. Eng. Chem.* **2014**, *20*, 3919–3946. [CrossRef]
7. Hou, Q.F.; Zhou, Z.Y.; Yu, A.B. Discrete element modeling of gas fluidization of fine ellipsoidal particles. *AIP Conf. Proc.* **2013**, *1542*, 1130.
8. Widiawaty, C.D.; Siswantara, A.I.; Budiarso, B.; Daryus, A.; Gunadi, G.G.R.; Pujowidodo, H. Investigation the effect of superficial velocity to the heat transfer in bubbling regime of fluidization using CFD simulation. *AIP Conf. Proc.* **2019**, *2187*, 020024.
9. Behjat, Y.; Shahhosseini, S.; Hashemabadi, S.H. CFD modeling of hydrodynamic and heat transfer in fluidized bed reactors. *Int. Commun. Heat Mass Transf.* **2008**, *35*, 357–368. [CrossRef]
10. Uwitonze, H.; Kim, A.; Kim, H.; Brigljević, B.; Ly, H.V.; Kim, S.-S.; Upadhyay, M.; Lim, H. CFD simulation of hydrodynamics and heat transfer characteristics in gas–solid circulating fluidized bed riser under fast pyrolysis flow condition. *Appl. Therm. Eng.* **2022**, *212*, 118555. [CrossRef]
11. Cai, M.; Tian, Z.; Liu, Z.; Liu, B. A computational fluid dynamics model coupled with ethylene polymerization kinetics for fluidized bed polyethylene reactor. *Powder Technol.* **2022**, *407*, 117647. [CrossRef]
12. Tokmurzin, D.; Nam, J.Y.; Park, S.J.; Yoon, S.J.; Mun, T.-Y.; Yoon, S.M.; Moon, J.H.; Lee, J.G.; Lee, D.H.; Ra, H.W.; et al. Three-Dimensional CFD simulation of waste plastic (SRF) gasification in a bubbling fluidized bed with detailed kinetic chemical model. *Energy Convers. Manag.* **2022**, *267*, 115925. [CrossRef]
13. Chiesa, M.; Mathiesen, V.; Melheim, J.A.; Halvorsen, B. Numerical simulation of particulate flow by the Eulerian–Lagrangian and the Eulerian–Eulerian approach with application to a fluidized bed. *Comput. Chem. Eng.* **2005**, *29*, 291–304. [CrossRef]
14. Khawaja, H.A. CFD-DEM simulation of minimum fluidisation velocity in two phase medium. *Int. J. Multiphysics* **2011**, *5*, 89–99. [CrossRef]
15. Shao, Y.; Gu, J.; Zhong, W.; Yu, A. Determination of minimum fluidization velocity in fluidized bed at elevated pressures and temperatures using CFD simulations. *Powder Technol.* **2019**, *350*, 81–90. [CrossRef]
16. Hagh-Shenas-Lari, M.J.; Mostoufi, N. Effect of Temperature on Fluidization Regimes. *Chem. Eng. Technol.* **2014**, *37*, 1593–1599. [CrossRef]
17. Seo, M.W.; Goo, J.H.; Kim, S.D.; Lee, J.G.; Guahk, Y.T.; Rho, N.S.; Koo, G.H.; Lee, D.Y.; Cho, W.C.; Song, B.H. The transition velocities in a dual circulating fluidized bed reactor with variation of temperatures. *Powder Technol.* **2014**, *264*, 583–591. [CrossRef]
18. Kiran, N.; Ekinci, E.; Snape, C.E. Recyling of plastic wastes via pyrolysis. *Resour. Conserv. Recycl.* **2000**, *29*, 273–283. [CrossRef]
19. Qureshi, M.S.; Oasmaa, A.; Pihkola, H.; Deviatkin, I.; Tenhunen, A.; Mannila, J.; Minkkinen, H.; Pohjakallio, M.; Laine-Ylijoki, J. Pyrolysis of plastic waste: Opportunities and challenges. *J. Anal. Appl. Pyrolysis* **2020**, *152*, 104804. [CrossRef]
20. Sieradzka, M.; Rajca, P.; Zajemska, M.; Mlonka-Mędrala, A.; Magdziarz, A. Prediction of gaseous products from refuse derived fuel pyrolysis using chemical modelling software—Ansys Chemkin-Pro. *J. Clean. Prod.* **2020**, *248*, 119277. [CrossRef]
21. Miandad, R.; Barakat, M.A.; Aburiazaiza, A.S.; Rehan, M.; Nizami, A.S. Catalytic pyrolysis of plastic waste: A review. *Process Saf. Environ. Prot.* **2016**, *102*, 822–838. [CrossRef]
22. Upadhyay, M.; Nagulapati, V.M.; Lim, H. Hybrid CFD-neural networks technique to predict circulating fluidized bed reactor riser hydrodynamics. *J. Clean. Prod.* **2022**, *337*, 130490. [CrossRef]
23. Kunii, D.; Levenspiel, O. *Fluidization Engineering*, 2nd ed.; Butterworth-Heinemann: Stoneham, MA, USA, 1991.
24. Asys Inc. *ANSYS Fluent Tutorial Guide*, 18th ed.; Ansys: Canonsburg, PA, USA, 2017.
25. De la Flor-Barriga, L.A.; Rodríguez-Zúñiga, U.F. Numerical analysis on a catalytic pyrolysis reactor design for plastic waste upcycling using CFD modelling. *RSC Adv.* **2022**, *12*, 12436. [CrossRef]
26. *Ansys® Granta EduPak*, Relese 2021 R2; Ansys: Canonsburg, PA, USA, 2022.
27. Kurniawati, D.; Putra, N.; Abdullah, N.; Hakim, I.I.; Nurrokhmat, A. An experimental analysis of diesel fuel produced from HDPE (high-density polyethylene) waste using thermal and catalytic pyrolysis with passive heat pipe cooling system. *Therm. Sci. Eng. Prog.* **2021**, *23*, 100917. [CrossRef]
28. Upadhyay, M.; Kim, A.; Kim, H.; Lim, D.; Lim, H. An Assessment of Drag Models in Eulerian-Eulerian CFD Simulation of Gas-Solid Flow Hydrodynamics in Circulating Fluidized Bed Riser. *ChemEngineering* **2020**, *4*, 37. [CrossRef]
29. Martínez, L.; Aguado, A.; Moral, A.; Irusta, R. Fluidized bed pyrolysis of HDPE: A study of the influence of operating variables and the main fluidynamic parameters on the composition and production of gases. *Fuel Process. Technol.* **2011**, *92*, 221–228. [CrossRef]
30. Abbasi, M.R.; Shamiri, A.; Hussain, M.A. A review on modeling and control of olefin polymerization in fluidized-bed reactors. *Rev. Chem. Eng.* **2019**, *35*, 311–333. [CrossRef]
31. Schwaiger, K.; Haider, M.; Hämmerle, M.; Wünsch, D.; Obermaier, M.; Beck, M.; Niederer, A.; Bachinger, S.; Radler, D.; Mahr, C.; et al. SandTES—An active thermal energy storage system based on the fluidization of powders. *Energy Procedia* **2014**, *49*, 983–992. [CrossRef]
32. Schneiderbauer, S.; Puttinger, S.; Pirker, S.; Aguayo, P.; Kanellopoulos, V. CFD modeling and simulation of industrial scale olefin polymerization fluidized bed reactors. *Chem. Eng. J.* **2015**, *264*, 99–112. [CrossRef]
33. Entrée, E.B. Fluidized Bed. 2011. Available online: https://www.thermopedia.com/content/46/ (accessed on 16 August 2022).

34. Cal Chem Corporation, CHE 435: Fluidized Bed Characteristics. Available online: https://www.cpp.edu/ (accessed on 16 August 2022).
35. Eder, C.; Hofer, G.; Pröll, T. Wall-to-Bed Heat Transfer in Bubbling Fluidized Bed Reactors with an Immersed Heat Exchanger and Continuous Particle Exchange. *Ind. Eng. Chem. Res.* **2021**, *60*, 7417–7428. [CrossRef]